Received: 25 June 2022 | Revised: 5 December 2022 | Accepted: 6 December 2022

DOI: 10.1002/rcs.2491

ORIGINAL ARTICLE

The International Journal of Medical Robotics and Computer Assisted Surgery

WILEY

Virtual-force-guided intraoperative ultrasound scanning with online lesion location prediction: A phantom study

Baoshan Niu[1] | Dapeng Yang[1,2] | Peng Wang[1] | Haonan Yang[1,2] | Le Zhang[1] | Yikun Gu[1] | Li Jiang[1]

[1]State Key Laboratory of Robotics and System, Harbin Institute of Technology, Harbin, China

[2]Artificial Intelligence Laboratory, Harbin Institute of Technology, Harbin, China

Correspondence
Yikun Gu, State Key Laboratory of Robotics and System, Harbin Institute of Technology, Harbin, 150001, China.
Email: guyikun@hit.edu.cn

Funding information
Interdisciplinary Research Foundation of HIT, Grant/Award Number: IR2021218; Postdoctoral Scientific Research Development Fun, Grant/Award Number: LBH-W18058; The NSF Grant, Grant/Award Number: 52075114

Abstract

Background: In ultrasound-guided minimally invasive surgery (MIS) of tumours, it is crucial to discover the optimal scanning plane (OSP) and organise the MIS scalpel work trajectory in this plane. The OSP can be altered and is challenging to track when the scalpel interacts with deformed tissues. Therefore, tracking the OSP becomes critical in MIS. In master-slave control, virtual force (VF) is used to assist the operator in completing the task. However, most literature assumes that the environment is sufficiently stable. No specific method focuses on tracking the OSP of the lesion within largely deformed tissues.

Methods: This paper used the improved artificial potential field method to establish the VF that could guide the operator to track the OSP. When tissue deformation occurred, an artificial neural network (ANN) was used to predict the target position, guiding the operator to find the new OSP. An experimental robot platform was built to verify the proposed algorithm's effects. Experiments to track the OSP were performed on a phantom.

Results: The results showed that the presented method could reduce the trajectory redundancy of ultrasonic scanning, shorten the time of OSP discovery and tracking, and decrease the deviation between the ultrasonic scanning position and the OSP.

Conclusions: This method has significance for the accurate localization and successful removal of tumours. Future work will focus on improving the adaptability of the proposed ANN prediction model in different phantoms.

KEYWORDS
intraoperative ultrasound scanning, lesion location prediction, minimally invasive surgical robot, virtual force

1 | INTRODUCTION

As one of the primary diseases, cancer will soon replace heart disease to become the world's leading killer, seriously threatening human health.[1] The principal cancer treatments include surgery, chemotherapy, and radiation,[2] in which surgical removal of the tumours is the most effective way. MRI, X-ray, CT, and ultrasound are generally applied for image guidance during resection.[3] MRI provides superior contrast between soft tissues but cannot be used for real-time imaging. Moreover, the electronics stop working in strong magnetic fields. X-ray and CT cannot provide real-time imaging and are associated with a certain amount of radiation. Ultrasound is one of the mainstream medical imaging devices due to its flexibility, ease of integration, and ability to image in real-time.[4,5]

Although ultrasound imaging has the above advantages, it is necessary to empirically adjust the imaging parameters according to

the properties of the imaging target and select the appropriate imaging plane by adjusting the probe pose.[6] Surgeons do not widely use ultrasound equipment due to their long learning curve and high cognitive load.[7] Ultrasound-guided minimally invasive surgery (MIS) of tumours puts forward stricter requirements on ultrasound scanning, which requires scanning the lesion in the ultrasound image and finding the OSP (one of the three-dimensional symmetry planes or the quasi-three-dimensional symmetry planes of the lesion). The scalpel axis will deviate from the lesion's centre if the operator does not insert the scalpel in the OSP. Furthermore, the tumours will be destroyed during the feeding and withdrawal of the scalpel, resulting in residual tumours and even hastening the spread of cancer, causing severe damage to patients.

The virtual force (VF) guides the ultrasound scanning plane to align with the OSP and control the scalpel puncture in the OSP. The force-guided technique is widely used in master-slave operations to reduce physical isolation between surgeons and patients.

2 | LITERATURE REVIEW

As illustrated in Table 1, the research on virtual-force-assisted master-slave control was divided into three categories in this article: (1) assisting the tool in reaching a specific target, (2) assisting the instrument in moving along the desired path, and (3) restricting the surgical instrument to a specific area or limit access to a specific area.

2.1 | Assisting the tool in reaching a specific target

James found that force assistance in master-slave control could improve manipulation accuracy, simplify task internalization, and allow more efficient communication between operators' brain neurons.[8,9] The VF was generated based on the gaze point, and the operator tracked the marked points on the beating heart with the VF. Gibo discovered that force guidance could promote the learning of motor skills and help subjects adopt preferable strategies.[10] However, the above methods cannot be used for force guidance during ultrasound scanning because the lesions are hidden inside the tissue and cannot be observed.

2.2 | Assisting the instrument in moving along the desired path

Liu proposed a master-slave control scheme to aid cataract capsulorhexis surgery. Based on the simulated work path and the current position of the surgical instruments, the attractive force was calculated and fed back to the master control terminal to ensure that the instruments were on the correct path.[11] Xiong developed a modified artificial potential field (APF) method to create guidance paths and provide haptic guidance at the master.[12] Abayazid used ultrasound imaging and path planning to compute the desired needle orientation during insertion and passed the information to the operator, who teleoperated the motion of the needle's tip.[13] The above three methods use VF to assist master-slave control in improving the tracking accuracy of the desired path. A precise path cannot be determined before the ultrasound scan of the lesion in the deformed soft tissue.

2.3 | Restricting the surgical instrument to a specific area or limits access to a specific area

A relatively common approach in the literature is to use a high-precision 3D model of the anatomy in a virtual environment to constrain the robot's motion.[14] Marinho employed a virtual fixture to improve stitching performance.[15] He also approximated the complex-shaped nasal cavity with a truncated cone.[16] Simple measurements could obtain an approximately truncated cone before surgery. The movement of the instrument was restricted within the truncated cone. Hong proposed a forbidden region virtual fixture developed to assist in simulation-based laparoscopic surgery training.[17] Rossi presented a novel master-slave telerobotic haptic system for stereotactic neurosurgery.[18] Most virtual fixtures with fixed shapes are used in the above research. The shape of the virtual fixture comes from preoperative CT or MRI image data. However, this does not apply to this study because the scalpel puncture will move the lesion's location.

2.4 | Conclusions of the literature review

To reach a specific target, the VF is related to the Euclidean distance between the current position and the target. If tracking a specific

TABLE 1 Overview of virtual-force-assisted master-slave control

References	Main approach	Advantages	Disadvantages
8,9,10	Assisting the tool in reaching a specific target	Simplify task internalization; promote skill learning	Most literature assumes the environment is stable enough
11,12,13	Assisting the instrument in moving along the desired path	Improved path tracking accuracy	
14,15,16,17,18	Restricting the instrument to a specific area or limits access to a specific area	Prevent vital organs from being broken	
	The proposed method	Adjust the virtual force according to lesion's position	Require equipment to measure the deformation

path, the VF is associated with Euclidean distance and its first and second derivatives. If the surgical instrument is restricted to a specific area or limits access to a specific area, the VF is related to the Euclidean distance between the current position of the instrument and the area boundary. These three situations attract the current point to a low-energy place. The APF could transform the existing environment of the robot into an energy field and guide it to a low-potential energy point.

In the literature surveyed, few papers consider 'active dynamic constraints'. 'Active dynamic constraint'means that the geometry of the constraint is constantly changing due to environmental changes. Most literature assumes that the environment is stable enough to use static constraints. Unfortunately, the VF cannot adapt to the unstructured environment. The operation area will be deformed, and the trajectory will be shifted when the surgical instruments act on human organs or tissues. Therefore, it is challenging to apply the pre-calculated virtual guiding forces to the soft tissue.[19] Research on active dynamic constraints on soft tissue is a major challenge.[20]

To remove the tumour in the soft phantom, the scalpel must be punctured to the location of waiting for cutting and then cut and remove the lesion. One of the lesion's three-dimensional symmetrical planes is selected as the OSP (the OSP is defined in 3.1.3). To prevent the scalpel axis from deviating and destroying the lesion during cutting, the first step is to locate the OSP of the lesion and align the ultrasound scanning plane with it. The second step is to puncture the scalpel in the OSP plane. This paper focuses on finding and tracking the OSP of the lesion in a deformed phantom.

As shown in Figure 1, the scalpel puncture is performed when the ultrasound scan plane coincides with the OSP plane of the lesion. The lesions and the OSP of the lesion in the phantom will move due to puncture force. Therefore, it becomes necessary to move the ultrasound probe to a new position where the plane of the probe can coincide with the OSP of the lesion.

The VF studied in this paper can adapt to an unstructured environment. Firstly, the improved APF technology was used to create a VF to assist the operator in finding the lesion's OSP for the first time. Secondly, the puncture of the scalpel would cause a change in the position of the target point in the APF. In order to make the ultrasonic scanning plane track the OSP in real-time during surgical puncture, the position of the target point was predicted by the artificial neural network (ANN). The VF was updated based on the predicted new target point location. Finally, the evaluation indicators were established to verify the effectiveness of the proposed strategy integrating APF and ANN. Three comparative experiments were conducted: (1) without VF, (2) with VF, and (3) with VF and ANN.

3 | MATERIALS AND METHODS

3.1 | System settings

This section focuses on system settings, which include the experimental platform, preparation for the hydrogel phantom, and the definition of the target point (P_t) and OSP.

3.1.1 | Experimental platform

The experimental platform is shown in Figure 2. The system includes the ultrasound image display module, the teleoperation module, the MIS scalpel module, and the robotic table. SonoStar's wireless probe is used for scanning. Force Dimension Omega.7 (left and right) is used for master-slave control. UR3 is applied for mounting the probe, and UR5 is utilised to hold the MIS scalpel. The surgical procedure for removing lesions is as follows: first, the operator holds the Omega.7 (left) to control the ultrasound scanning robot. Then, the ultrasound probe contacts the surface of the phantom. An ultrasound image is formed and displayed on the screen. Moreover, according to the ultrasound image, the operator uses Omega.7 (right) to control the scalpel robotic arm to puncture the phantom in the preset position and perform tumour cutting and removal.

Minimally invasive scalpel resection of the lesion is divided into three steps[21]: puncture, excision, and parcel, as shown in Figure 3. The elastic metal sheet is hidden in the tube at the beginning of the puncture, and a sharp puncture blade is installed to reduce the resistance (Figure 3A). In Figure 3B, C_2D_2 is the long axis of the ellipsoidal lesion. Position H, collinear to the long axis of the lesion and 2 mm from D_2, is defined as the position waiting for cutting. The minimally invasive scalpel is punctured to position H to be cut under the guidance of the ultrasonic image. The elastic metal sheet stretches out, and the energised metal wire begins to cut the tissue (Figure 3C). A shrapnel cavity surrounds the lesion (Figure 3D-1). Figure 3D-2 demonstrates that the axis of the scalpel is deflected from the centre of the lesion. If the lesion is cut in this situation, it will be cut into two parts: the red

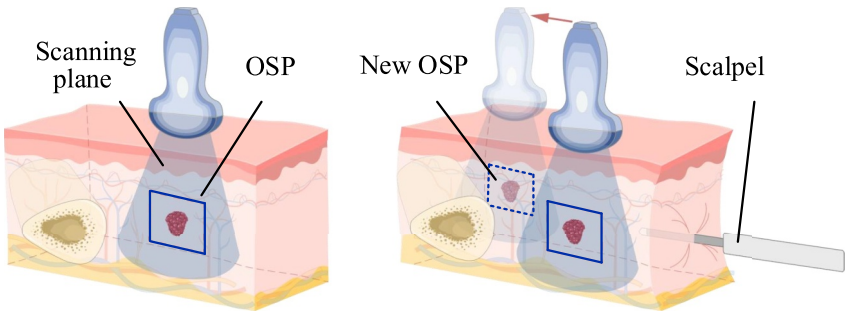

FIGURE 1 Tracing the lesion's optimal scanning plane (OSP) by moving ultrasonic probe.

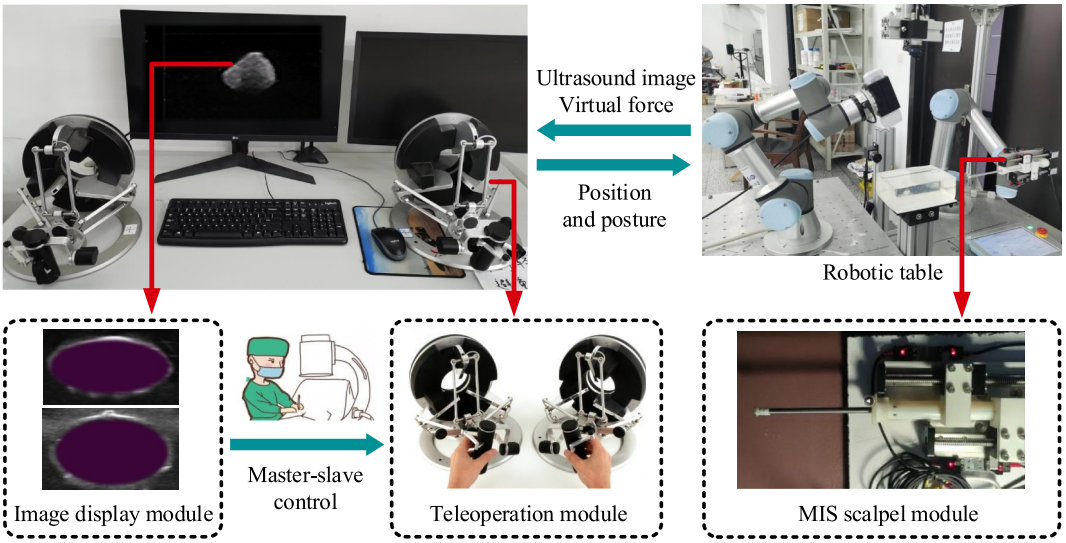

FIGURE 2 The minimally invasive surgery (MIS) robot platform.

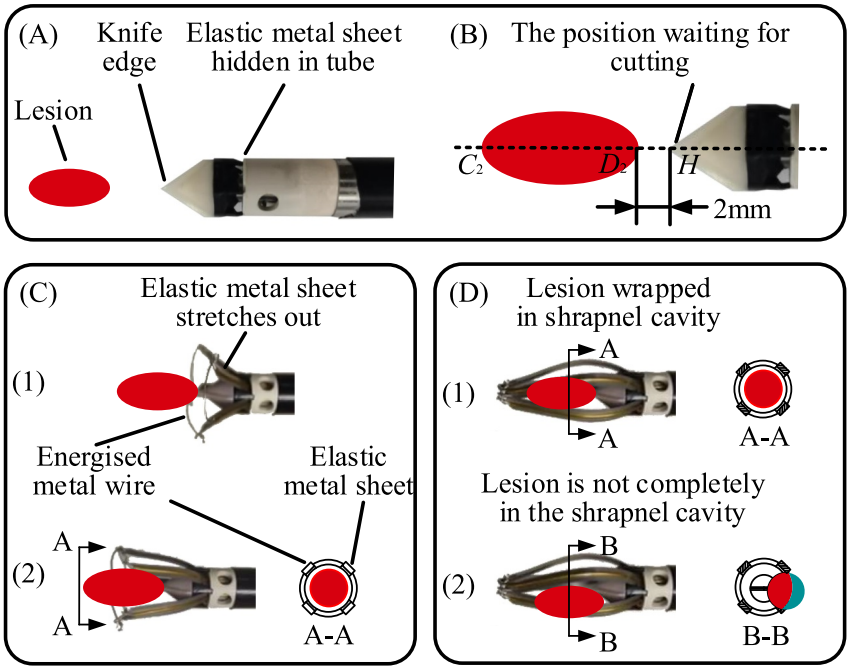

FIGURE 3 Steps for cutting lesions with the minimally invasive scalpel. (A), (B) puncture; (C) excision; (D) parcel.

part and the green part (B-B view of Figure 3D-2). The red component is wrapped in the cartridge cavity. The green component is not removed. The above situation may destroy the lesion and cause the tumour to spread, so it should be avoided.

3.1.2 | Preparation for hydrogel phantom

The polyvinyl alcohol (PVA) hydrogel phantom was made according to.[22] The preparation method is shown in Table 2. The robot can cut and remove the tumours in the breast, abdominal, and thoracic cavities. Without loss of generality, the mixed liquid was poured into a rectangular model. The phantom was made into a rectangular shape. Before making the phantom, an ellipsoid (made of silica gel) was placed to simulate the tumours. Repeated freeze-thawing methods improved the tensile strength and transparency of the

TABLE 2 Preparation method for hydrogel phantom

Material	PVA	Deionized water	Dimethyl sulfoxide
Proportion	8 g	40 ml	60 ml
Conditions	Mix in proportion, heat and stir at 90°C–95°C for 3–5 h		

phantom. The freezing temperature was −20°C. The thawing temperature was room temperature.

3.1.3 | Definition of the target position (P_t) and the OSP

The poses of the two robot arms in Figure 2 are defined as the starting position (P_s), and the robot arms move from P_s during the experiment.

Breast cysts and fibromas are more prevalent in breast tumours and have an ellipsoidal or nearly ellipsoidal form. Lipomata are also a common benign tumour in soft tissue, and the shape is also ellipsoidal or approximately ellipsoidal. There is soft tissue, such as fat, around the lesion.

The planes that pass through the long axis A_1B_1 of ellipsoidal lesions are three-dimensional symmetric planes (1, 2, 3, 4, etc.), as shown in Figure 4A. The point on the phantom surface closest to the lesion's centre (O_1) is defined as the initial target position (P_t), where the normal of the phantom surface is $\vec{n}$. Among the numerous three-dimensional symmetric planes, parallel or coplanar with $\vec{n}$ is defined as OSP (plane 4 in Figure 4A). As shown in Figure 4B, in most cases, the lesion's shape is irregular, and then the minimum external ellipsoid of the lesion is found first. P_t and OSP are then determined by the minimum external ellipsoid.

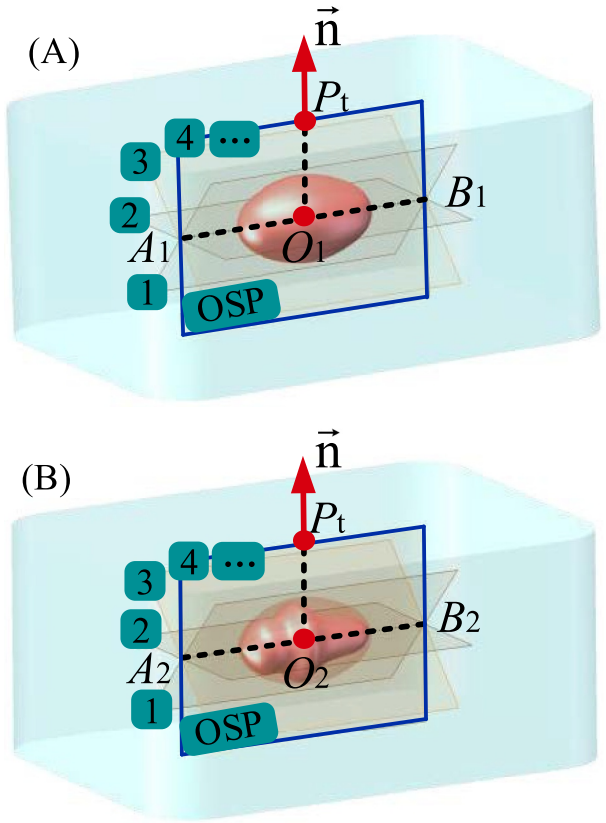

FIGURE 4 The definition of P_t and the optimal scanning plane (OSP). (A) ellipsoidal lesion; (B) irregular lesion.

3.2 | Virtual-force-guidance based on the improved APF

In this section, the improved APF technology was used to create a VF to assist the operator in finding the lesion's OSP for the first time.

The APF is a virtual-force-based method for robot path planning with smooth paths and high search efficiency.[23] The APF contains attractive and repulsive fields. The lesion in soft tissue without surrounding blood vessels and organs was removed in this experiment. Therefore, only an attractive field was established.

The traditional attractive field was

$$U_{att} = \frac{1}{2}\xi\rho^2(P_n, P_t) \tag{1}$$

where $\rho(P_n, P_t)$ is the distance between the current position and the target position; ξ is the attraction coefficient.

The attraction is the derivative of the attractive field to distance. There is a large attractive force when the object is away from the target. The attraction field was adjusted, and the influence distance d_0 was added to avoid excessive attraction force. When the distance was far from the target, the attraction was prevented from being too large, as shown in Equations (2) and (3).

$$U_{att} = \begin{cases} \frac{1}{2}\xi\rho^2(P_n, P_t) & \rho(P_n, P_t) \le d_0 \\ d_0\xi\rho(P_n, P_t) - \frac{1}{2}\xi d_0^2 & \rho(P_n, P_t) > d_0 \end{cases} \tag{2}$$

$$F_{att} = \begin{cases} \xi\rho(P_n, P_t) & \rho(P_n, P_t) \le d_0 \\ d_0\xi & \rho(P_n, P_t) > d_0 \end{cases} \tag{3}$$

As shown in Figure 5, during the movement of the ultrasonic probe from P_s to P_t, the phantom does not deform because there is no insertion of the scalpel. In the above process, the switch is connected to 0.

The VF based on the APF is as follows: preoperative CT or MRI data is used to identify the shape and position of the lesion. Then the position of P_t (x_t, y_t, z_t) can be obtained. The current position P_n (x_n, y_n, z_n) of the ultrasonic probe is obtained by reading the state of the UR3 robot. $F_{slave\text{-}1}$ and $F_{master\text{-}1}$ are the virtual forces at the slave (UR robot) and master, respectively, from the initial position to first find the OSP. When P_n and P_t are known, $F_{slave\text{-}1}$ is calculated according to Equation (4). $F_{master\text{-}1}$ can be calculated from $F_{slave\text{-}1}$, as shown in Equation (5).

$$F_{slave-1} = \begin{cases} \xi\rho(P_n, P_t) & \rho(P_n, P_t) \le d_0 \\ d_0\xi & \rho(P_n, P_t) > d_0 \end{cases} \tag{4}$$

$$F_{master-1} = k \cdot F_{slave-1} \tag{5}$$

where k is the scale factor.

$F_{master\text{-}1}$ is fed back to the teleoperated via a coordinate transformation. Under master-slave control assisted by $F_{master\text{-}1}$, the ultrasonic probe reaches the initial target position (the x, y, and z

positions of the probe are determined). Generally, the *z*-axis of the ultrasonic probe is kept collinear with the normal of the contact surface during scanning (the *x* and *y* directions of the probe are determined), and then the operator rotates around the *z*-axis of the probe to align the scanning plane with the OSP.

It is noteworthy that the six degrees of freedom of the manipulator are master-slave controlled by the operator, and the VF generated by the APF only assists the master-slave operation.

As shown in Figure 5, after the ultrasound probe moves to P_t, the MIS scalpel begins to puncture the phantom. The lesion position moves with the puncture of the MIS scalpel (P_t will also move to P'_t (x'_t, y'_t, z'_t)). The target position will shift posteriorly if the operation area is anatomically symmetrical. Therefore, the OSP remains unchanged, as shown in Figure 6A. However, in general, the anatomy of the area is not symmetrical, and there may be constraints such as bones, which make it challenging to determine the target location and the OSP, as shown in Figure 6B. Consequently, it is necessary to study the deformation modelling of soft tissue.

3.3 | Predict the displacement of P'_t and update the virtual force

The puncture of the scalpel will cause a change in P_t in the APF. In order to make the ultrasonic scanning plane track the OSP in real-time during surgical puncture, the position of P'_t was predicted by ANN. The VF was updated based on the predicted location of P'_t.

There are two approaches to modelling soft tissue deformation: (1) biomechanical-based methods, and (2) statistical-based methods. Modelling based on biomechanics utilises physical knowledge, which is computationally complex. The calculation takes approximately ten seconds to a few minutes or even longer.[24,25] Therefore, it is challenging to meet real-time needs.

Therefore, a statistical-based modelling approach was applied, as shown in Figure 5. In the above process, the switch was connected to 0. Four markers were posted on the surface of the experimental phantom.

Eight Vicon cameras measured the displacement of the marking points in real time. The displacement of four markers P_i (x_i, y_i, z_i)

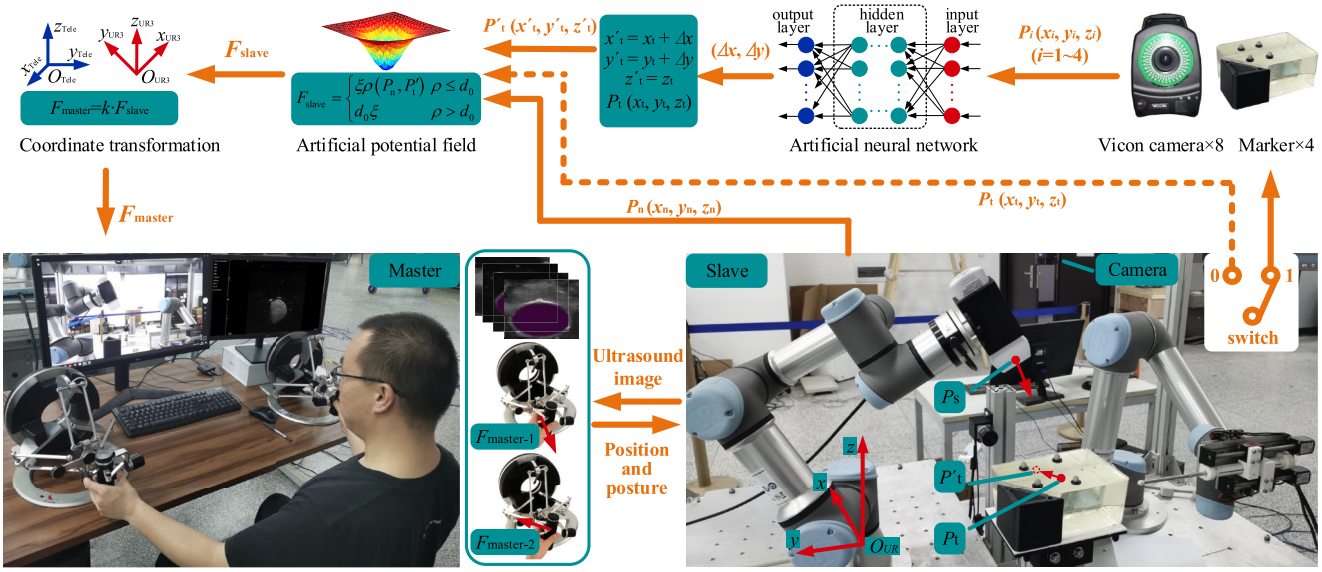

FIGURE 5 Virtual-force-guided intraoperative ultrasound scanning with online lesion location prediction on a phantom.

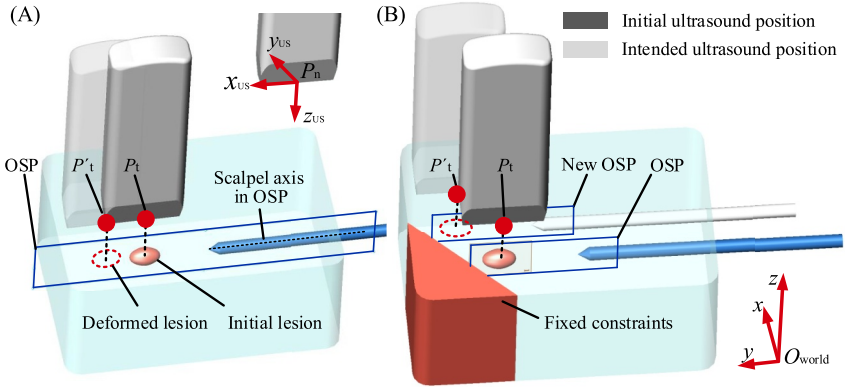

FIGURE 6 Lesion location changes during puncture with minimally invasive surgery (MIS) scalp. (A) anatomical symmetry; (B) anatomical asymmetry.

(i = 1–4) was the input of the ANN. The displacement of the target point in the xoy plane (Δx, Δy) was the output of the ANN.

Then, P'_t (x'_t, y'_t, z'_t) was obtained according to Equation (6).

$$\begin{cases} x'_t = x_t + \Delta x \\ y'_t = y_t + \Delta y \\ z'_t = z_t \end{cases} \tag{6}$$

The target point of the ultrasonic probe was on the upper surface of the model, that is, $z'_t = z_t$. Therefore, the ANN did not need to predict Δz (because $\Delta z \equiv 0$), only needed to predict and output Δx and Δy.

$F_{slave\text{-}2}$ and $F_{master\text{-}2}$ are the virtual forces at the slave (UR robot) and master, respectively. According to P'_t and P_n, $F_{slave\text{-}2}$ is calculated according to Equation (7) and updated in real time. $F_{master\text{-}2}$ can be calculated from $F_{slave\text{-}2}$, as shown in Equation (8)

$$F_{slave-2} = \begin{cases} \xi\rho(P_n, P_t') & \rho(P_n, P_t') \le d_0 \\ d_0\xi & \rho(P_n, P_t') > d_0 \end{cases} \tag{7}$$

$$F_{master-2} = k \cdot F_{slave-2} \tag{8}$$

The operator performed an ultrasound scan based on the image and $F_{master\text{-}2}$, as shown in Figure 5.

In this process, the six degrees of freedom of the manipulator are master-slave controlled by the operator, and the updated VF based on ANN only serves to assist the master-slave operation.

In order to predict the displacement (Δx, Δy) of the target point in the xoy plane and obtain the position of P'_t, the following researches need to be carried out: (1) firstly, obtaining the samples, (2) then, training the ANN, and (3) finally, prediction of the target location online and updating the VF.

3.3.1 | Obtaining samples

The equipment for obtaining samples is shown in Table 3. The experimental phantom's upper surface is parallel to the xoy plane, and the target point's motion is also in this plane, as shown in Figure 5. Only the x and y direction deformations need to be predicted. The displacement in the x and y directions of the lesion centre was measured by a camera above the phantom. The hydrogel phantom was made transparent to simplify the measurement. As shown in Figure 6, the x and y coordinate values of P'_t and the centre of the lesion were equal.

TABLE 3 Equipment for obtaining samples

Equipment	Vicon	Basler acA1600-60gm
Functions	Measuring the displacement of the markers	Measuring the displacement in x and y directions of the lesion centre
Precision	0.15 mm	0.2 mm

The scalpel was driven by the UR5 and punctured the lesion. The markers displacement P_i (x_i, y_i, z_i) (i = 1–4) and the target displacement Δx, Δy were recorded. The obtained sample size was 298.

3.3.2 | Training ANN

The mathematical theory demonstrates that feedforward networks with a single hidden layer containing a finite number of neurons can approximate any nonlinear continuous function in the original spatial interval.[26] The backpropagation neural network was selected to predict the nonlinear deformation model of soft tissue.

The principle was to minimise the mean square error between the actual output value and the predicted value using the gradient descent method to make backpropagation adjustments to the weights and thresholds.

The samples were randomly selected 70% for training, 15% for validation, and 15% for testing. There were 12 input layer neurons, which were $[X_1, X_2, X_3, X_4, \dots, X_{12}] = [x_1, y_1, z_1, x_2, \dots, z_4]$. The output layer neurons were 2 in total, $[Y_1, Y_2] = [\Delta x, \Delta y]$. The number of neurons in the hidden layer was determined according to the following formula[27]:

$$n_h = \sqrt{n_i + n_o} + a \tag{9}$$

where n_h is the number of neurons in the hidden layer; n_i and n_o are the number of neurons in the input and output layers, respectively, and a is 1–10.

There was a sigmoidal activation function in the hidden layer and a linear activation function in the output layer. The function was trained using the gradient descent adaptive learning rate.

To verify the accuracy of the ANN, 35 new samples were selected for validation. Figure 7 shows the predicted and measured values in the x and y directions, respectively. The displacement of the target position in the Δx and Δy directions can be accurately predicted by the ANN. The maximum error in the x direction is 0.398 mm, and the average error is 0.143 mm. The maximum error in the y direction is 1.26 mm, and the average error is 0.233 mm.

3.3.3 | Prediction the target location online and updating the virtual force

Each trained ANN layer's connection weights and bias values were loaded into the project engineering file. The Vicon measured the displacements of the four markers. ANN predicted the target position, and the calculation took less than 1 ms. The frequency of the Vicon online measurement was 50 Hz. Therefore, the total time from data measurement to lesion location prediction would be at most 21 ms by this method. Theoretically, after successfully predicting the target position with the ANN, the robot could autonomously scan and locate the OSP of the lesion. Nevertheless, there would be errors in the predicted target position based on the ANN, and there were

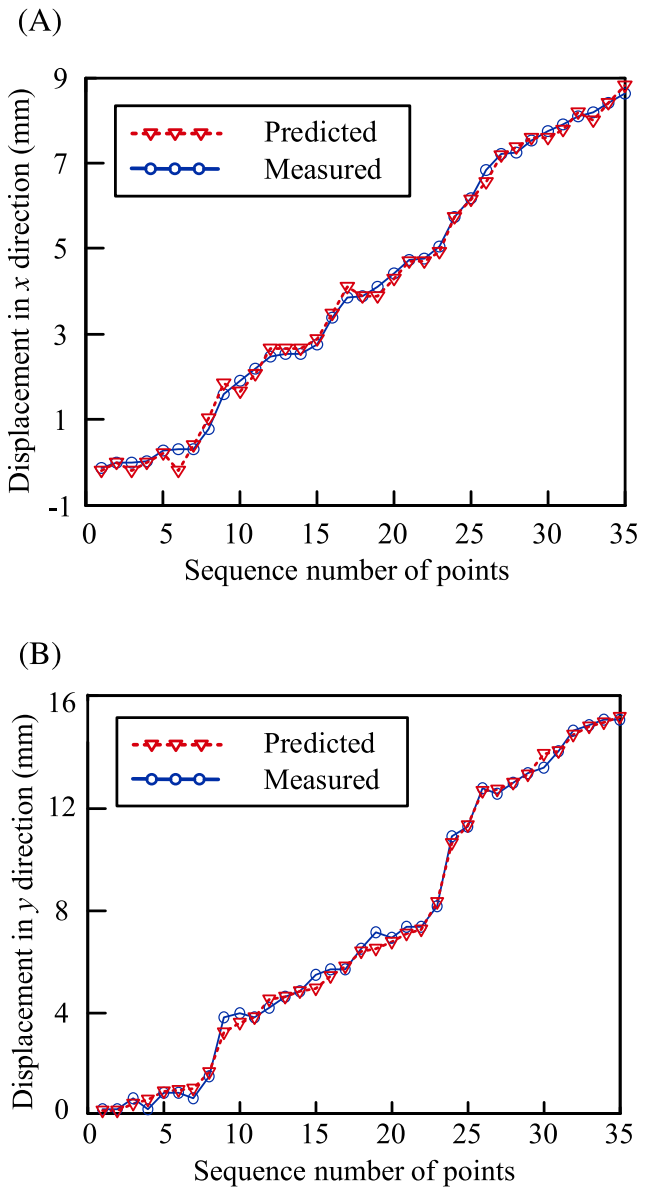

FIGURE 7 The comparison between the experimentally measured target position displacement and the predicted results by artificial neural network (ANN). (A) Displacement in *x* direction. (B) Displacement in *y* direction.

problems with its safety and reliability during autonomous surgery. Surgical robots are the least intelligent among robots, so the master-slave control approach is necessary.[28]

3.4 | Evaluation metrics

To evaluate the quality of the operator's ultrasound scanning task, the ultrasonic scanning trajectory redundancy (TR), the time of discovering and tracking the OSP, and the ratio of lesion area in the ultrasound scan plane to that in the OSP plane were selected as evaluation indicators.

(1) The TR of ultrasonic scanning can be calculated in Equation (10), which describes how close the real trajectory is to the ideal trajectory. The closer they are to each other, the less redundant they are[29]

$$TR = \frac{L_r}{L_s} \tag{10}$$

where L_r is the length of the real trajectory (the green trajectory in Figure 12A,C,E); L_s is the length of the shortest path (the blue trajectory in Figure 12A,C,E). $L_s = P_sP_t + P_t P'$.

(2) The time of discovering and tracking the OSP.

(3) The ratio of the lesion area in the ultrasound scan plane (S_1) to that in the OSP plane (S_2). The value of S_1/S_2 represents the deviation of the ultrasound scanning position from the OSP.

As shown in Figure 8, A-A is the lesion in the ultrasound scan plane, and the area is denoted as S_1; B-B is the lesion in the OSP, with an area of S_2. The distance between the ultrasonic scanning plane and OSP is *d*. In the experiment, the value of *d* is not easy to measure. However, *d* is related to S_1/S_2. The closer S_1/S_2 is to 1, the closer *d* is to 0, and the closer the ultrasonic scanning plane is to OSP. The closer S_1/S_2 is to 0, the larger *d* is, and the farther the ultrasonic scanning plane is from the OSP.

To fully describe the process of ultrasonic probe adjustment during puncture as well as reduce data processing, three images considered as the most oversized lesion contours were collected during the puncture process. The first image was collected without puncture, the second was obtained when the puncture reached 1/2, and the third was assembled when the puncture was completed.

After completing the image acquisition, the image was measured offline, and the length of the lesion's long axis (C_1D_1) and short axis (E_1F_1) was measured in the software named WirelessUSG. Then S_1 was obtained according to Equation (11). Because the size of the lesion was artificially defined, C_2D_2 and E_2F_2 were known, and then S_2 was obtained according to Equation (12).

$$S_1 = C_1D_1 \cdot E_1F_1 \cdot \pi/4 \tag{11}$$

$$S_2 = C_2D_2 \cdot E_2F_2 \cdot \pi/4 \tag{12}$$

4 | EXPERIMENTS AND RESULTS

To verify the effectiveness of the proposed virtual-force-guidance strategy integrating APF and ANN, three groups of comparative experiments were set up: (1) ultrasound scan without VF (baseline, BL), (2) ultrasound scan with VF, and (3) ultrasound scan with VF and ANN deformation prediction (VFANN).

Each group performed 16 punctures, and at the beginning of each experiment, the ultrasound probe and the scalpel were returned to their initial positions.

4.1 | Ultrasound scan without virtual force (baseline, BL)

Figure 9 shows that when VF is unavailable, the manipulator's TR is the highest and the most dispersed. Figure 10 indicates that when there is no VF, the time for discovering and tracking the OSP is the longest. Later, with the number of experiments increasing, the operator's proficiency increased, and the time spent gradually decreased and finally stabilized. As seen in Figure 11, without VF, the value of S_1/S_2 on the 1st, the 2nd, and the 3rd ultrasound scans is the smallest. The values do not differ significantly between the groups.

Figure 12A demonstrates that when no VF moves from the starting point to the initial target, the working trajectory deviates from the ideal trajectory. When the operator remotely controls the ultrasound probe to reach the phantom's upper surface, the operator does not know the lesion's location and shape in advance. The operator must move the ultrasound probe in an extensive range to construct the lesion location and shape information and find the OSP. Figure 12B indicates that it takes nearly 120 s to find the OSP for the first time, and the moving range along the *x* direction is [−230, −160] mm. During the following puncture of the scalpel, with the lesion position moving, the operator still has to move the probe and construct the lesion position and shape information. It takes 70 and 50 s to find the OSP for the second and the third time, respectively. The movement range in the *x* direction is [−210, −175] mm. Massive time is wasted finding the OSP for ultrasound, and the ultrasound scan trajectories near the target are the densest.

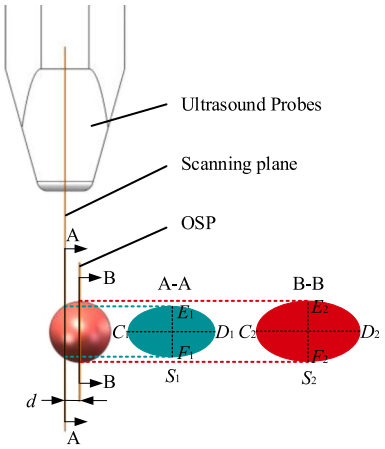

FIGURE 8 Ratio of lesion area in ultrasound scan plane (S_1) to that in optimal scanning plane (OSP) plane (S_2).

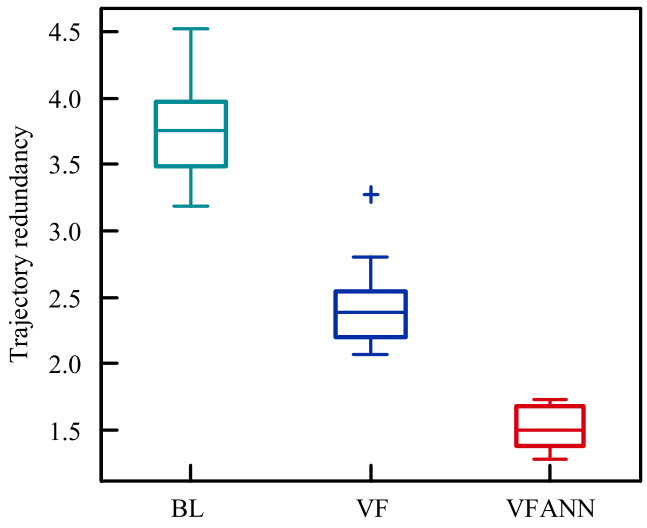

FIGURE 9 The trajectory redundancy (TR) of ultrasonic scanning.

4.2 | Ultrasound scan with virtual force

Figure 9 shows that when there is VF, the TR of the manipulator decreases. However, there is an abnormal value of 3.27, which may be caused by the incorrect placement of the phantom in this experiment. The target point set in the APF is inconsistent with the phantom. During the first scan, the VF did not directly guide the operator to the OSP position. Moreover, the operator had to

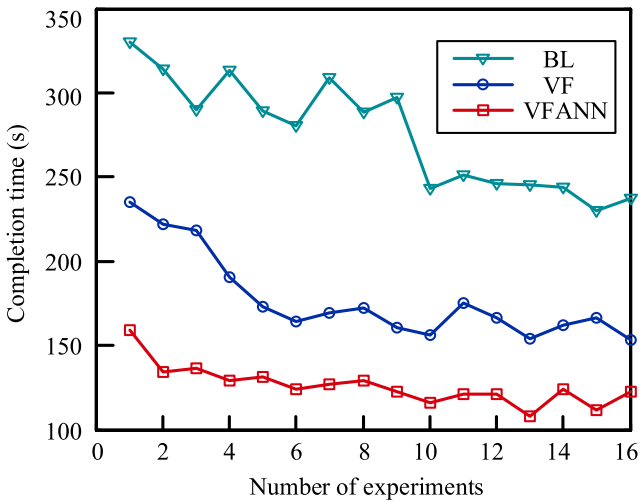

FIGURE 10 The time of discovering and tracking the optimal scanning plane (OSP).

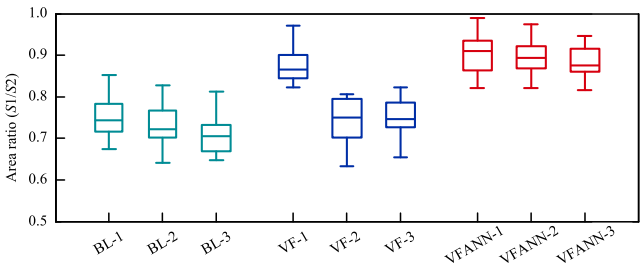

FIGURE 11 Ratio of lesion area in ultrasound scan plane (S_1) to that in optimal scanning plane (OSP) plane (S_2). '−1', '−2', '−3' represent the 1st, the 2nd and the 3rd ultrasound scan.

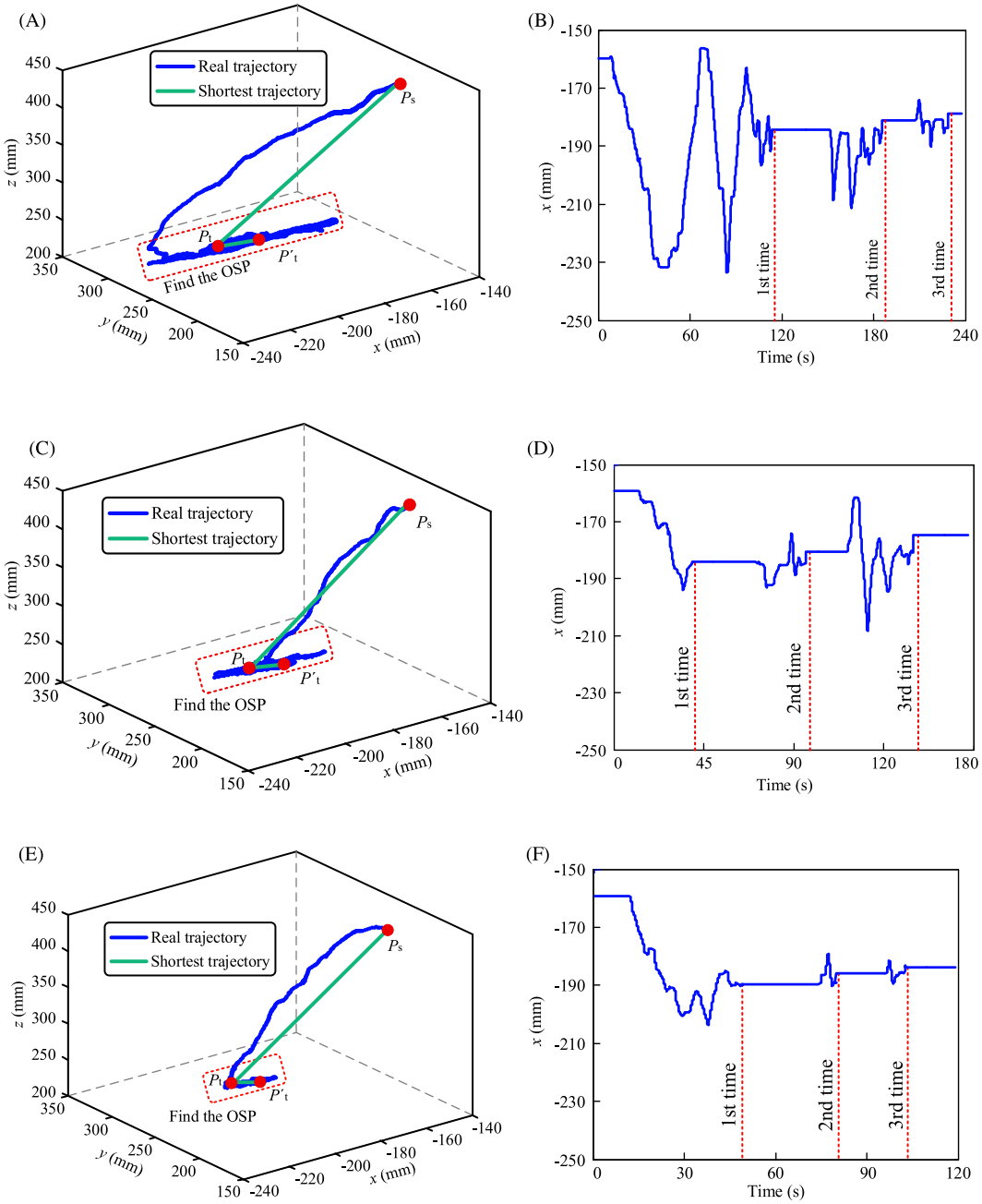

FIGURE 12 Comparison of ultrasound scanning arm trajectories in 3 groups. (A) BL-3D trajectory (B) BL-*x*-direction trajectory. (C) VF-3D trajectory (D) virtual force (VF) -*x*-direction trajectory. (E) VFANN-3D trajectory (F) VFANN -*x*-direction trajectory.

determine the OSP without VF empirically. Figure 10 indicates that after the virtual guiding force is added, the time for discovering and tracking the OSP is significantly reduced. In Figure 11, the median of the value of S_1/S_2 on the 1st, the 2nd, and the 3rd ultrasound scans is 0.87, 0.75, and 0.74, respectively, when VF is available. The value of S_1/S_2 in the first ultrasound scan image was more significant than in the last two, indicating that the first ultrasound scan plane was closest to the OSP. The above analysis is proper because the first scan is to reach the preset target position.

Figure 12C shows that when VF is available, the trajectory is closer to the theoretical trajectory. With the virtual guiding force, the ultrasonic probe moves directly to the initial target position and quickly locates the OSP. However, when the scalpel punctures, the lesion position moves. The operator needs to move the probe, construct information on the position and spatial shape of the lesion according to the ultrasound image, and then discover the position of the OSP. Therefore, in the same group of experiments, the value of S_1/S_2 of the first scan is greater than the value of S_1/S_2 of the second and third scans. By comparing Figure 12B,D, it is found that the virtual guiding force can reduce the moving range of the ultrasonic probe along the *x* direction, thereby reducing the time to first find the OSP.

TABLE 4 Comparison between our method and biomechanical-based methods

	Time complexity	Storage complexity	Pre-processing	Post-processing	Running time
Biomechanical-based method	O ($n \times m$)	O ($n \times m$)	O(m)	O(m)	14110 ms (7872 nodes, 1000 steps)
The proposed method	O (1)	O (1)	O (1)	O (1)	21 ms

4.3 | Ultrasound scan with virtual force and ANN deformation prediction (VFANN)

As seen in Figure 9, with VF and ANN deformation prediction, the robotic arm has the lowest TR and the densest data distribution, indicating that the operator performs the most stable task. It can be seen from Figure 10 that when there is VF and ANN deformation prediction, the time of discovering and tracking the OSP is the least. Figure 11 shows that with VF and deformation prediction, the value of S_1/S_2 in the 1st, the 2nd, and the 3rd ultrasound scans are the largest. With a median between 0.87 and 0.91, there is no significant difference between the values of the groups.

Figure 12E,F show that the target can be predicted in the 1st, the 2nd, and the 3rd ultrasonic scans when VF and deformation prediction are added. It avoids moving the ultrasound probe in an extensive range in the x direction to find the OSP of the lesion, and the time of discovering and tracking the OSP is the least.

4.4 | Comparison of computational complexity

Table 4 compares the complexity and computational time of the ANN statistical-based and biomechanical-based methods.[30] The method based on biomechanics can accurately obtain the deformation field of soft tissue and the displacement of each discrete point in the model. However, obtaining accurate results requires many nodes (m, thousands to tens of thousands) and calculation steps (n, thousands to tens of thousands), so the calculation is enormous and the required time is long. The method based on statistics needs some prior samples, and the algorithm complexity is slight. However, if the model changes, it will be necessary to collect new samples and retrain the network. In this study, we need to ensure real-time calculation only to predict the location of the target point. Therefore, it is reasonable to use the data-based modelling method.

5 | CONCLUSIONS AND FUTURE WORK

In order to locate the lesion's three-dimensional centre and prevent the minimally invasive scalpel from deviating from the centre, this paper is the first study on tracking the lesion's OSP in deformable tissue. Firstly, the concept of OSP for lesions was proposed. After that, the APF technique was employed to create a VF, which was fed back to the ultrasound operator to help trace the OSP quickly and accurately. Considering that the OSP would change due to the MIS scalpel operation, the ANN was employed to predict the new lesion location. The virtual guidance force was updated in real-time to align the probe's scanning plane with the OSP.

Significantly, the median of the TR of the ultrasonic scanning manipulator was reduced by 60.3% with VF and deformation prediction. The average time required to determine the OSP was reduced by 54.9%. The median value of S_1/S_2 on the 1st, the 2nd, and the 3rd ultrasound scans was increased by 24.7%, 26.8%, and 24.3%, respectively. The conclusion was summarised as follows: in light of the VF and tissue deformation prediction, our method could lower the TR of the ultrasound scanning robot and reduce the burden of discovering and tracking the OSP. Moreover, it could increase the ratio of the detected lesion area to its theoretical maximum in ultrasound images (that is, it could improve the closeness of the scanning plane to the OSP), which was crucial in profiling an internal lesion and conducting MIS. The OSP, where the scalpel is punctured, is accurately positioned, making a complete lesion cut and removal possible. The limitation of the proposed method is that it needs to use Vicon to measure the displacement of the four markers, which is prone to deviations in the measurement due to light occlusion. In addition, eight cameras will also occupy a large space. The smaller NDI Polaris Vega ST can be used to measure the markers. Our future research will focus on the generalisation of the soft tissue prediction model and the study of MIS scalpel puncture under ultrasound guidance.

ACKNOWLEDGEMENT

This work was supported by the National Natural Science Foundation of China (52075114), Interdisciplinary Research Foundation of HIT (IR2021218), and Postdoctoral Scientific Research Development Fun (LBH-W18058) to D. Yang.

CONFLICT OF INTEREST

The authors declare that they have no known competing financial interests or personal relationships that could have appeared to influence the work reported in this paper.

DATA AVAILABILITY STATEMENT

The data that support the findings of this study are available on request from the corresponding author. The data are not publicly available due to privacy or ethical restrictions.

ORCID

Baoshan Niu https://orcid.org/0000-0003-2523-0729

REFERENCES

1. Siegel RL, Miller KD, Jemal A. Cancer statistics, 2020. *CA-Cancer J Clin*. 2020;70(1):5-29. https://doi.org/10.3322/caac.21590

2. Barui S, Cauda V. Multimodal decorations of mesoporous silica nanoparticles for improved cancer therapy. *Pharmaceutics*. 2020; 12(6):1-2. https://doi.org/10.3390/pharmaceutics12060527
3. Gillies DJ, Bax J, Barker K, Gardi L, Kakani N, Fenster A. Geometrically variable three-dimensional ultrasound for mechanically assisted image-guided therapy of focal liver cancer tumourss. *Med Phys*. 2020; 47(10):1-3. https://doi.org/10.1002/mp.14405
4. Haxthausen FV, Bttger S, Wulff D, Hagenah J, Garcia-Vazquez V, Ipsen S. Medical robotics for ultrasound imaging: current systems and future trends. *Curr Robot Rep*. 2021;2(1):55-71. https://doi.org/10.1007/s43154-020-00037-y
5. Deng X, Lei Z, Wang Y, et al. Learning ultrasound scanning skills from human demonstrations. *Sci China Inf Sci*. 2021;1–9(8):184201. https://doi.org/10.1007/s11432-021-3363-0
6. Ning GC, Zhang XR, Liao HE. Multi-degree-of-freedom intelligent ultrasound robot system based on reinforcement learning. *J Electron Inf Technol*. 2022;44(01):1-10.
7. Wang TM, Zhang XH, Zhang XB, et al. Research progresses in laparoscopic augmented reality navigation. *Robot*. 2019;41(01):124-136.
8. James DRC, Leff DR, Orihuela EF, et al. Enhanced frontoparietal network architectures following "gaze-contingent" versus "free-hand" motor learning. *Neuroimage*. 2013;64:267-276. https://doi.org/10.1016/j.neuroimage.2012.08.056
9. Mylonas GP, Kwok KW, James D, et al. Gaze-contingent motor channelling, haptic constraints and associated cognitive demand for robotic MIS. *Med Image Anal*. 2012;16(3):612-631. https://doi.org/10.1016/j.media.2010.07.007
10. Gibo TL, Abbink DA. Movement strategy discovery during training via haptic guidance. *IEEE Trans Haptics*. 2016;9(2):243-254. https://doi.org/10.1109/toh.2016.2516984
11. Liu W, Su Y, Wu W, Xin C, Hou ZG, Bian GB. An operating smooth man–machine collaboration method for cataract capsulorhexis using virtual fixture. *Future Generat Comput Syst*. 2019;98:522-529. https://doi.org/10.1016/j.future.2019.01.032
12. Xiong LF, Chng CB, Chui CK, Yu P, Li Y. Shared control of a medical robot with haptic guidance. *Int J Comput Assist Radiol Surg*. 2017;12(1): 1-11. https://doi.org/10.1007/s11548-016-1425-0
13. Abayazid M, Pacchierotti C, Moreira P, Alterovitz R, Prattichizzo D, Misra S. Experimental evaluation of co-manipulated ultrasound-guided flexible needle steering. *Int J Comput Assist Radiol Surg*. 2016; 12(2):219-230. https://doi.org/10.1002/rcs.1680
14. Heredia-Pérez SA, Harada K, Padilla-Castaeda MA, et al. Virtual reality simulation of robotic transsphenoidal brain tumours resection: evaluating dynamic motion scaling in a master-slave system. *Int J Comput Assist Radiol Surg*. 2019;15(1).
15. Marinho MM, Ishida H, Harada K, Deie K, Mitsuishi M. Virtual fixture assistance for suturing in robot-aided pediatric endoscopic surgery. *IEEE Rob Autom Lett*. 2020;5(2):524-531. https://doi.org/10.1109/lra.2019.2963642
16. Marinho MM, Harada K, Morita A, Mitsuishi M. Smartarm: integration and validation of a versatile surgical robotic system for constrained workspaces. *Int J Comput Assist Radiol Surg*. 2019;16(2). https://doi.org/10.1002/rcs.2053
17. Hong M, Rozenblit JW. A haptic guidance system for computer-assisted surgical training using virtual fixtures. In: *IEEE International Conference on Systems*. IEEE; 2017.
18. Rossi A, Trevisani A, Zanotto V. A telerobotic haptic system for minimally invasive stereotactic neurosurgery. *Int J Comput Assist Radiol Surg*. 2005;1(2):64-75. https://doi.org/10.1581/mrcas.2005.010209
19. Selvaggio M, Fontanelli GA, Ficuciello F, Villani L, Siciliano B. Passive virtual fixtures adaptation in minimally invasive robotic surgery. *IEEE Rob Autom Lett*. 2018;3(4):3129-3136. https://doi.org/10.1109/lra.2018.2849876
20. Bowyer SA, Davies BL, Baena F. Active constraints/virtual fixtures: a survey. *IEEE Trans Robot*. 2014;30(1):138-157. https://doi.org/10.1109/tro.2013.2283410
21. Allen SD, Nerurkar A, Della Rovere GUQ. The breast lesion excision system (BLES): a novel technique in the diagnostic and therapeutic management of small indeterminate breast lesions? *J. Eur radiol*. 2011;21(5):919-924. https://doi.org/10.1007/s00330-010-2000-7
22. Liu XY. *Research of Trajectory Planning of Needle Insertion in Soft Tissue Based on Potential Field Method and Experiment Validation, Dissertation for the Master Degree*. Tianjin University; 2010;10–21.
23. Li P, Jiang S, Liang D, Yang Z, Yu Y, Wang W. Modeling of path planning and needle steering with path tracking in anatomical soft tissues for minimally invasive surgery. *Med Eng Phys*. 2017;41:35-45. https://doi.org/10.1016/j.medengphy.2017.01.006
24. Davatzikos C, Shen D, Mohamed A, Kyriacou S. A framework for predictive modeling of anatomical deformations. *IEEE Trans Med Imag*. 2001;20(8):836-843. https://doi.org/10.1109/42.938251
25. Zhou JY, Lou Z, Li CQ, Deng M. Real-time deformation of human soft tissues: a radial basis meshless 3D model based on Marquardt's algorithm. *Comput Methods Progr Biomed*. 2018;153:237-252. https://doi.org/10.1016/j.cmpb.2017.09.008
26. Goodfellow I, Bengio Y, Courville A. *Deep Learning*. MIT press; 2016: 194-197.
27. Zou FL, Leng S, Lian PF, et al. An improved method on determining the reasonable number of hidden nodes of BP neural network. *Syst Simulat Technol*. 2017;10(2):154-158.
28. Simorov A, Otte RS, Kopietz CM, Oleynikov D. Review of surgical robotics user interface: what is the best way to control robotic surgery? *Surg Endosc*. 2012;26(8):2117-2125. https://doi.org/10.1007/s00464-012-2182-y
29. Xing Y, Niu SK, Jin K, et al. Evaluation of robot-assisted surgery skills based on EM-GRA. *J Tianjin Univ*. 2021;54(06):636-644.
30. Zhang J, Chauhan S. Fast computation of soft tissue thermal response under deformation based on fast explicit dynamics finite element algorithm for surgical simulation[J]. *Comput Methods Progr Biomed*. 2020;187:105244. https://doi.org/10.1016/j.cmpb.2019.105244

SUPPORTING INFORMATION

Additional supporting information can be found online in the Supporting Information section at the end of this article.

How to cite this article: Niu B, Yang D, Wang P, et al. Virtual-force-guided intraoperative ultrasound scanning with online lesion location prediction: a phantom study. *Int J Med Robot*. 2022;e2491. https://doi.org/10.1002/rcs.2491